

# Bayesian Model Selection of Lithium-Ion Battery Models via Bayesian Quadrature<sup>★</sup>

Masaki Adachi<sup>\*,\*\*</sup> Yannick Kuhn<sup>\*\*\*,\*\*\*\*</sup>  
 Birger Horstmann<sup>\*\*\*,\*\*\*\*</sup> Michael A. Osborne<sup>\*</sup>  
 David A. Howey<sup>\*\*,†</sup>

<sup>\*</sup> Machine Learning Research Group, University of Oxford, OX2 6ED, UK (e-mail: masaki@robots.ox.ac.uk).

<sup>\*\*</sup> Battery Intelligence Lab, University of Oxford, OX1 3PJ, UK

<sup>\*\*\*</sup> German Aerospace Center (DLR), Pfaffenwaldring 38-40, 70569 Stuttgart, Germany

Helmholtz Institute Ulm, Helmholtzstraße 11, 89081 Ulm, Germany

<sup>\*\*\*\*</sup> Universität Ulm, Albert-Einstein-Allee 47, 89081 Ulm, Germany

<sup>†</sup> The Faraday Institution, Harwell Campus, Didcot OX11 0RA, UK

---

**Abstract:** This paper presents a Bayesian model selection approach via Bayesian quadrature and sensitivity analysis of the selection criterion for a lithium-ion battery model. The Bayesian model evidence is adopted as the metric, which can select the simplest but well-describing model based on Occam’s razor principle. While the model evidence requires prohibitive integral computations over parameter space, Bayesian quadrature offers sample-efficient integration via model-based inference to minimise the number of battery model evaluations. The posterior distribution of battery model parameters can also be inferred as a byproduct in one go, which is also beneficial in creating a digital twin. The simplest lithium-ion battery models, equivalent circuit models, were used to analyse the sensitivity of the selection criterion at given different datasets and model configurations. We show that popular selection criteria, such as root-mean-square error, and Bayesian information criterion, can fail to select a correct model in a multimodal posterior case. The model evidence can spot the true model in such cases, simultaneously providing the variance of evidence inference itself as an indication of confidence. Bayesian quadrature can compute the evidence faster than popular MCMC solvers.

---

**Keywords:** Bayesian methods, identifiability, parameter estimation, battery, lithium-ion

---

## 1. INTRODUCTION

The lithium-ion battery is key to decarbonising power grids and electrifying vehicles as an impactful climate action. However, its voltage-current response is non-linear in principle and challenging to model, control, and diagnose, which is a practical hindrance to exploiting the most out of its performance. Furthermore, the high capacity benefit of lithium-ion batteries is associated with their drawback of explosive aspect, requiring safety-first control. Moreover, the available dataset obtained from batteries is typically limited to three dimensions; voltage, current, and temperature. Estimating the internal state from these time-varying three variables is challenging or even mathematically impossible for many response patterns due to parameter identifiability issues (Bizeray et al., 2018). In addition, degradation worsens matters since the number of parameters to be identified becomes larger when considering long-term ageing data, requiring the decomposition of stationary and non-stationary factors.

There are dozens of plausible electrochemical models for Li-ion batteries, owing to differing assumptions or levels of approximation. While electrochemists prefer complicated models such as the Doyle-Fuller-Newman model (Doyle et al., 1993) for an academic understanding of internal chemical reactions and transport, control engineers prefer simpler models such as equivalent circuit models (ECMs) (He et al., 2011), for fast control and fewer parameters. Other models exist in a spectrum between the above simple and complex models (simple, ECM < EHM (Milocco et al., 2014) < SPM (Santhanagopalan et al., 2006) < SPMe (Kemper and Kum, 2013) < DFN, complex). System identification is the foundation of an estimation and control system, determining predictive accuracy, quick response, and reliability.

However, the ‘best’ model should be ascertained based on quantifiable performance metrics. Importantly, the best model strongly depends on the dataset  $\mathbf{D}$  and user requirements. The widely accepted metric defining ‘good’ models would be Occam’s razor, in which the simplest model to reasonably reproduce the given dataset is considered the best. Simplesness here means the number of parameters to be identified. Rasmussen and Ghahramani (2000) showed such a metric could be evaluated via Bayesian model

---

<sup>★</sup> This work has been submitted to IFAC for possible publication. Code is publicly available at: <https://github.com/Battery-Intelligence-Lab/BayesianModelSelection>

evidence. The evidence can be obtained by integrating out the parameters  $\theta$  from the likelihood:

$$p(\mathbf{D}|M) = \int_{\chi} p(\mathbf{D}|\theta, M) dp(\theta), \quad (1)$$

where  $p(\theta)$  is the prior distribution,  $p(\mathbf{D}|\theta, M)$  is the likelihood. The mean evidence  $\mathbb{E}_{\chi}[p(\mathbf{D}|M)]$  gives the probability of reproducing a given dataset  $\mathbf{D}$  with a given model  $M$ . The evidence quantifies Occam's razor and is widely accepted as the best metric for Bayesian model selection. Moreover, the evidence is a probability distribution. While the mean gives the degree of model fit, the variance quantifies the uncertainty about the fit.

Surprisingly, Bayesian model selection on battery models has barely been reported, despite an explosion in battery modelling literature. To the best of our knowledge, Miyazaki et al. (2020) is the only previous work that applied Bayesian model selection to battery models. While Bayesian parameter estimation (Aitio et al., 2020; Escalante et al., 2021), and probabilistic modelling works (Huang et al., 2021; Liu and Ciucci, 2020) exist, they do not go beyond parameter estimation. Most Bayesian works in the battery community are performed with sample-inefficient Markov chain Monte Carlo (MCMC) (Metropolis et al., 1953; Hastings, 1970) due to user-friendliness. Although recent work (Kuhn et al., 2022) applied a sample-efficient solver with Bayesian optimisation, none of the above solvers offer evidence computation. This is because evidence computation requires prohibitive integral computation, which is challenging, particularly when the likelihood is non-closed-form and/or expensive, such as the simulator-based likelihood we face. A typical practice in such cases is to adopt the Bayesian information criterion (BIC), which is a coarse approximation of the evidence, assuming the posterior is a unimodal Gaussian. However, the battery parameter estimation can produce multimodal or non-Gaussian (Aitio et al., 2020; Escalante et al., 2021) posterior distributions. Mis-assumption causes overconfidence. In fact, the previous work (Miyazaki et al., 2020), based on a variant of BIC, failed to spot the true model in the hardly identifiable case.

This paper introduces Bayesian quadrature (BQ) for sample-efficient evidence *and* posterior estimation. Adachi et al. (2022) proposed a state-of-the-art Bayesian quadrature method that permits parallelisation for speed and also provides the posterior distribution of battery model parameters as a byproduct, which is also beneficial in system identification. We improved upon this work to accommodate a wider dynamic range of likelihood. We adopted ECMs for demonstration, analysis, and comparison with existing works applied to synthetically generated datasets. We also derived a canonical form of ECMs for statistical analysis.

## 2. BATTERY MODEL FORMULATION

We selected ECMs for proof-of-concept as the simplest model to analyse the BQ behaviours. ECM identifiability is typically examined with impedance spectra in a frequency regime, called electrochemical impedance spectroscopy (EIS). Several plausible ECMs are often compared for analysing EIS based on an electrochemical understanding of the target battery. For simplicity, we chose

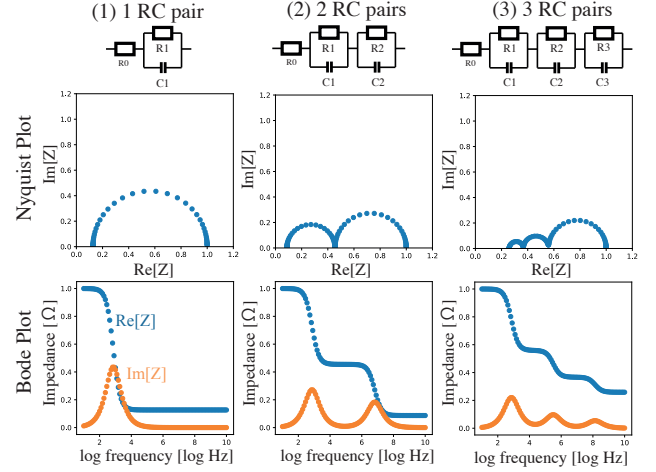


Fig. 1. Model selection from three RC pair models.

the resistance-capacitance (RC) pair model. Figure 1 illustrates the circuit configurations and typical Nyquist plot of selected three models. The impedance response of batteries can be approximated as a capacitor with leakage current in terms of an electric circuit. The number of RC parallel connection components corresponds to the number of the half circles in the Nyquist plot. This correspondence is key in identifying the model from spectra. As this perfect half-circle shape implies, the real and imaginary parts of spectra have a mathematical relationship. In dielectric physics, this relationship is well-known as Debye relaxation, meaning one part of spectra can derive the other via the equation.

We extend this formulation to make the model friendly for statistical inference, termed the canonical form of ECMs. Calderwood (2003) showed Debye relaxation could be written as hyperbolic functions. We improved the formulation upon their work, permitting non-dimensionalised parameterisation without positivity constraint, formulated as:

$$\text{Re}[Z] = P_{\text{re}} \left[ r_0 + \sum_{i=1}^N \frac{r_i}{2} [1 - \tanh(\tau_i)] \right], \quad (2)$$

$$\text{Im}[Z] = \underbrace{P_{\text{im}}}_{\text{scaling factor}} \underbrace{\left[ \sum_{i=1}^N \frac{w_i}{\pi} \text{sech}(\tau_i) \right]}_{\text{mixture of hyperbolic secant distributions}}, \quad (3)$$

where

$$P_{\text{re}} := \sum_{i=0}^N R_i := R_{\text{total}} := \exp(r_t), \quad (4)$$

$$P_{\text{im}} := R_{\text{total}} \frac{\pi(1 - r_0)}{2}, \quad (5)$$

$$r_i := \frac{R_i}{R_{\text{total}}} := \exp[-\exp(r'_i)], \quad (6)$$

$$r_0 := 1 - \sum_{i=1}^N r_i, \quad w_i := \frac{r_i}{1 - r_0}, \quad (7)$$

$Z$  is the complex impedance,  $\text{Re}[Z]$  and  $\text{Im}[Z]$  is the real and imaginary parts of the impedance spectra, respectively,  $R_0$  is the direct current (DC) resistance  $[\Omega]$ ,  $R_i$  is the resistance of  $i$ -th RC-pair  $[\Omega]$ ,  $w_i$  is the weight of  $i$ -th hyperbolic secant distribution corresponding to the  $i$ -th

RC-pair,  $N$  is the number of RC-pairs,  $\tau_i = \ln(\omega R_i C_i)$  is the logarithmic time constant of  $i$ -th RC-pair,  $\omega := 2\pi f$  is the angular frequency [rad/s],  $f$  is the frequency [Hz],  $C_i$  is the capacitance of  $i$ -th RC-pair [F],  $r_i$  is the dimensionless resistance of  $i$ -th RC-pair,  $r'_i$  is the unconstrained dimensionless resistance of  $i$ -th RC-pair.

This canonical form provides three-fold benefits; separation of scaling factor, unconstrained prior distribution selection, and integral-friendly formulation. Separating scaling factors can decompose parameter estimation problems into the problems of estimating magnitude and ratio, permitting fair comparison over the varied magnitude of resistance. Logarithmically transformed parameters can unlock the non-negativity constraints over resistance, allowing arbitrary prior distribution for Bayesian inference. A mixture of hyperbolic secant distribution formulation offers several integral identities to analytically calculate the expectation and variance. Moreover, this formulation can interpret the imaginary part as a probability distribution function, allowing statistical analysis.

The frequency range is also standardised via given frequency dataset, as such:

$$\mu_\omega, \sigma_\omega := \mathbb{E}[\ln \omega], \sqrt{\mathbb{V}\text{ar}[\ln \omega]}, \quad (8)$$

$$\omega^{\text{std}}, \tau_i^{\text{std}} := \frac{\ln \omega - \mu_\omega}{\sigma_\omega}, -\frac{\ln \tau'_i + \mu_\omega}{\sigma_\omega}, \quad (9)$$

$$\tau_i := \ln \omega \tau'_i = \ln \omega - \sigma_\omega \tau_i^{\text{std}} - \mu_\omega, \quad (10)$$

$$C_i = \frac{\tau'_i}{r_i R_{\text{total}}}. \quad (11)$$

The mean  $\mu_\omega$  and standard deviation  $\sigma_\omega$  of logarithmic angular frequency  $\ln \omega$  can be calculated from the given frequency range of the dataset,  $\tau_i^{\text{std}}$  is the standardised time constant.

### 3. BAYESIAN INFERENCE FORMULATION

We wish to select the likeliest model from the above three RC pairs. In Bayesian inference, we need to assume the inference model, consisting of prior distribution  $p(\Theta) := \pi(\Theta)$  and the likelihood function  $p(\mathbf{D}|\Theta, M) := \ell_{\text{true}}(\Theta)$ . The prior distribution is a probability distribution that reflects your belief in possible parameters. For instance, we adopted a multivariate normal distribution  $\pi(\Theta) := \mathcal{N}(\Theta; \mu_\pi, \Sigma_\pi)$ . While the mean vector  $\mu_\pi$  represents our guess of a plausible parameter set, the covariance matrix  $\Sigma_\pi$  reflects our uncertainty about each parameter and correlations between parameters. The likelihood function  $\ell_{\text{true}}(\Theta)$  is a probability distribution to reasonably evaluate how the selected parameter set  $\Theta$  can reproduce the given dataset  $\mathbf{D}$ . We assume a univariate Gaussian with a zero mean  $\mathbf{0}$  and a homoskedastic noise, meaning the noise variance  $\sigma_{\text{noise}}$  does not vary over frequency. The squared error evaluates how similar the observed data  $y_{\text{obs}}$  and ECM predicted data  $y_{\text{ecm}}$ . Now, with the assumed prior  $p(\Theta)$  and the likelihood function  $p(\mathbf{D}|\Theta, M)$ , Bayes' rule provides the parameter posterior  $p(\Theta, M|\mathbf{D})$  and the evidence  $p(\mathbf{D}|M)$ , in the form of:

$$p(\mathbf{D}|\Theta, M) := \ell_{\text{true}}(\Theta) := \prod_j^m \mathcal{N}(\text{err}_j(\theta); \mathbf{0}, \sigma_{\text{noise}}), \quad (12)$$

$$p(\mathbf{D}|M) := \mathcal{N}(\mathbb{E}_\pi[\ell_{\text{true}}(\Theta)], \mathbb{V}\text{ar}_\pi[\ell_{\text{true}}(\Theta)]), \quad (13)$$

$$p(\Theta|\mathbf{D}, M) = \frac{p(\mathbf{D}|\Theta, M)p(\Theta)}{p(\mathbf{D}|M)} = \frac{\ell_{\text{true}}(\Theta)\pi(\Theta)}{\mathbb{E}_\pi[\ell_{\text{true}}(\Theta)]}, \quad (14)$$

where

$$\mathbf{D} := \{\mathbf{y}_{\text{obs}}, \omega^{\text{std}}\} \in \mathbb{R}^{m \times 2}, \quad (15)$$

$$\theta := \{r_t, r'_i, \tau_i^{\text{std}}\} \in \mathbb{R}^{d-1}, \quad (16)$$

$$\Theta := \{\theta, \sigma_{\text{noise}}\} \in \mathbb{R}^d, \quad (17)$$

$$y_{\text{ecm},j}(\theta) := \{y_{\text{re},j}, y_{\text{im},j}\} = M(\theta, \omega_j^{\text{std}}), \quad (18)$$

$$\text{err}_j(\theta) := [y_{\text{obs},j} - y_{\text{ecm},j}(\theta)]^2. \quad (19)$$

The posterior  $p(\Theta, M|\mathbf{D})$  is a conditional probability distribution that reflects the updated belief of parameter space based on observed data  $\mathbf{D}$ . We use dimensionless and unconstrained  $r'_i$  and  $\tau_i^{\text{std}}$  as input of the model for arbitrary prior selection and fair comparison of models. The number of parameters to be estimated is  $d = 2 + 2N$ , as the scaling factor  $r_t$  and experimental noise variance  $\sigma_{\text{noise}}$  are shared over models.

### 4. BAYESIAN QUADRATURE MODELLING

We wish to estimate both the parameter posterior distribution  $p(\Theta, M|\mathbf{D})$  and the evidence  $p(\mathbf{D}|M)$ . At the same time, we wish to minimise the number of querying the likelihood  $\ell_{\text{true}}(\Theta)$ , as this can be a computationally demanding simulator. This problem requires a sample-efficient Bayesian inference solver. BQ can offer exactly the one which sample-efficiently solves the posterior and the evidence in one go. BQ is a surrogate-model-based numerical integration tool, solving the integral as an inference problem via modelling a likelihood function  $\ell_{\text{true}}(\Theta)$  with a Gaussian process (GP).  $\ell(\Theta)$  is the surrogate likelihood function modelled by GP. The key is that BQ can switch the problem of Bayesian inference into one of function approximation. As more accurately  $\ell(\Theta)$  can predict  $\ell_{\text{true}}(\Theta)$ , more accurately posterior and evidence can be estimated via replacing  $\ell_{\text{true}}(\Theta)$  with  $\ell(\Theta)$  in Eqs. (13) - (14). Adachi et al. (2022) proposed the discrete approximation of kernel integral using kernel recombination method (Hayakawa et al., 2022), termed *BASQ*, yielding the following evidence computations:

$$\log \mathbb{E}_\pi[\ell(\Theta)] \approx \log \sum_k^L W_k \mu_f(X_k) + \beta, \quad (20)$$

$$\log \mathbb{V}\text{ar}_\pi[\ell(\Theta)] \approx \log \sum_{k,l}^L W_k W_l \sigma_f(X_k, X_l) + 2\beta, \quad (21)$$

where  $\mu_f$  and  $\sigma_f$  are the predictive mean and covariance of the likelihood surrogate model  $\ell(\Theta)$ ,  $\beta$  is the scaling constant,  $W_k, W_l$  and  $X_k, X_l$  are the positive weights and point configurations discretised by the kernel recombination. However, their work assumed a narrower dynamic range of likelihood, whereas the battery model typically produces  $10^{700}$  likelihood values. This is way beyond the overflow limit. Thus, we improved their work by adopting four-layered warped GP methods to accommodate the wide dynamic range of likelihood. See Appendix A for more details.

## 5. IDENTIFIABILITY

We wish to evaluate the ability of the evidence for the model selection criterion. We adopted three quantities of classical metrics related to identifiability: the number of data points  $m$ , signal-to-noise ratio (SNR), and Kullback-Leibler divergence (KL). Thanks to the integral-friendly formulation, most parts can be calculated analytically. The number of data points is controllable because the data is synthetically generated, to be equispaced over log angular frequency space. Both SNR and KL are calculated using the imaginary part of the impedance. As the canonical form can be regarded as a mixture of hyperbolic secant distribution, such statistical analysis can be applied. While SNR evaluates the identifiability along the impedance magnitude axis, KL does so along the frequency axis.

### 5.1 Signal-to-Noise Ratio

SNR is the log fraction of the impedance variance over noise variance, representing how much the signal is more distinct than the noise, defined as:

$$\text{SNR} := \ln \frac{\text{Var}_{P(\ln \omega)}[\text{Im}[Z]]}{\sigma_{\text{noise}}}. \quad (22)$$

Therefore, larger SNR means a more distinct and more identifiable signal. Although it is defined as integration, the canonical form provides the analytical form of the solution. See derivation in Appendix B.2.

### 5.2 Kullback-Leibler Divergence

KL is a statistical distance of how one probability distribution  $P_i(x)$  is different from a second, reference probability distribution  $P_j(x)$ , defined as:

$$\text{KL} := \int_P \ln \left( \frac{P_i(x)}{P_j(x)} \right) dP_i(x) + \int_{P'} \ln \left( \frac{P_j(x)}{P_i(x)} \right) dP_j(x). \quad (23)$$

Typical KL definition is not symmetric against replacing the probability distributions  $P_i(x)$  and  $P_j(x)$ . Hence, we adopted symmetrised KL by adding up the replacement. As KL is defined for two distributions, the number of this criterion will increase combinatorially per the number of RC pairs. For simplicity, we only consider the case of two RC pairs, which produce only one KL. This represents how much the selected two peaks in imaginary parts overlap. Therefore, a larger KL means a more distinguishable and identifiable signal. As another point, this is formulated as noise-free. While SNR is determined by the noise variance  $\sigma_{\text{noise}}$  and scaling factor  $r_t$ , KL is dominated by the time constant difference  $\Delta\tau_{ij}$ . The canonical form helps solve integration. See derivation in Appendix B.3.

## 6. NUMERICAL RESULTS

### 6.1 Selection Criteria Comparison

We demonstrated our modified version of BASQ over several cases. We compare the metric with root-mean-square error (RMSE), Bayesian information criterion (BIC), and expected log predictive density (ELPD), based on the

Table 1. Easy case, LEM and LEV refer to log evidence mean and log evidence variance defined by Eqs. (20), (21), respectively

criterion	1 RC pair	2 RC pairs	3 RC Pairs
true model		✓	
LEM	-2809233	<b>703.6569</b>	289.2976
LEV	<b>-33.52068</b>	-27.31169	-31.91129
RMSE	1.147527	<b>0.006677</b>	0.031770
BIC	5766999	<b>-1405.553</b>	-572.7390
ELPD	-2883641	<b>713.7332</b>	293.2492

Table 2. Hard case

criterion	1 RC pair	2 RC pairs	3 RC Pairs
true model			✓
LEM	-150.3634	-151.8002	<b>-147.42566</b>
LEV	-15.74094	-19.07997	<b>-19.45956</b>
RMSE	<b>0.492191</b>	0.492643	0.492269
BIC	<b>302.86010</b>	313.89206	321.0089
ELPD	<b>-145.7505</b>	-148.8758	-148.4754

maximum a posteriori (MAP) estimation. The definitions are as follows:

$$\Theta_{\text{MAP}} := \text{argmax} \ell_{\text{true}}(\Theta), \quad (24)$$

$$\text{RMSE} := \sqrt{\frac{1}{m} \sum_j^m \text{err}_j(\theta_{\text{MAP}})}, \quad (25)$$

$$\text{BIC} := d \ln m - 2 \ln \ell_{\text{true}}(\Theta_{\text{MAP}}), \quad (26)$$

$$\text{ELPD} := \sum_j^m \ln \int_{\xi} \ell_{\text{true}}(\Theta) dp(\Theta | \mathbf{D}, M). \quad (27)$$

RMSE is a noise-free formulation that does not consider parameter uncertainty. BIC is an asymptotic approximation of evidence, so it cannot evaluate multimodal likelihood. ELPD is a similar formulation to the log mean evidence, but the probability measure is changed from prior  $\chi$  to posterior  $\xi$ . The motivation of ELPD is to estimate the alternative evidence from MCMC samples, as it cannot estimate evidence during solving Bayesian inference. However, it relies on Monte Carlo integration, which requires a significant amount of posteriors samples, meaning that a plethora of model evaluations  $\ell_{\text{true}}(\Theta)$  will run. All alternative criteria were calculated based on BQ estimated posterior as post-processing. Moreover, none of these criteria provides the uncertainty of their criteria, except BQ.

We demonstrated the behaviours of selection criteria on two different datasets. As expected from SNR and mutual information, separated peaks (large  $\Delta\tau_{ij}$ ) and lower noise  $\sigma_{\text{noise}}$  can boost the identifiability. Thus, we compared the following two cases: the easy case ( $\Delta\tau_{ij} = 9.1$ ,  $\ln \sigma_{\text{noise}} = -9.97$ ) in Table 1, and the hard case ( $\Delta\tau_{ij} = 0.36$ ,  $\ln \sigma_{\text{noise}} = -1.6$ ) in Table 2. While all criteria selected the true model in the easy case, only the evidence can select the true model in the hard case.

The other metrics were unsuccessful because of a multimodal posterior in the one RC pair model. As three RC pairs generate the dataset, the posterior distribution of one RC pair parameter inevitably becomes multimodal, such as peak intensity ( $w_i$ ). While the evidence correctly incorporate the multimodal distribution shape, RMSE and

Table 3. Linear correlation matrix

factors	$m$	KL	SNR	LEM	LEV
$m$	-	-0.0071	0.0058	0.4096	-0.1806
KL	-0.0071	-	-0.1166	0.0144	-0.2159
SNR	0.0058	-0.1166	-	0.7299	-0.4882
LEM	0.4096	0.0144	0.7299	-	-0.2867
LEV	-0.1806	-0.2159	-0.4882	-0.2867	-

BIC consider only the largest peak. BIC estimates the whole distribution from the local curvature at the maximum, which becomes erroneously overconfident in the multimodal case (Murphy, 2012). Moreover, BIC cannot judge the multimodality and parameter space compactness, leading to excessive reliance on the number of parameters  $d$ . ELPD’s failure could be due to the rough integral approximation. As the convergence rate of Monte Carlo integration is  $\mathcal{O}(1/\sqrt{n})$ , the number of posterior samples ( $n = 1,000$ ) is not enough for convergence. However, it means more model evaluations  $\ell_{\text{true}}(\Theta)$  are required. Thus, this judging criteria would not scale to the computationally demanding simulators.

In contrast, evidence can be estimated simultaneously during training. Moreover, the variance of evidence successfully pointed out the lower confidence in the one RC pair in the hard case, suggesting multimodality. This uncertainty over the selection criterion could avoid overconfidence toward a simpler model. Moreover, the evidence variance in the hard case is generally higher than in the easy case. This also tells that the hard case dataset is hardly identifiable, suggesting we should not trust these comparisons. For instance, the evidence mean and ELPD for one RC pair in the easy case are much lower than in the hard cases. However, the integral variance is the opposite. Thus, only this metric advises the metric uncertainty, suggesting the dataset or model is less informative. A similar notion can be found in Jeffreys’ scale for the Bayes factor (Jeffreys, 1998), which claims the evidence is not strong when the difference between the log evidence of two models is lower than 10. This explains that the hard case is unreliable, as the difference in the log evidence shows insufficient plausibility. Contrary to Jeffreys’ scale, log evidence variance is self-contained, which does not require the comparison of models. Instead, it can independently spot the unreliability of the estimation.

In such an uncertain case, a typical practice is Bayesian model averaging. Rather than selecting one definite model, we sample from a *mixture of models* with probability proportional to the mean evidence. Averaging can contribute to boosting predictive accuracy and reducing the uncertainty over prediction. By contrast, as BIC is not a probability, it cannot use for averaging weights. As such, while the easy cases do not require advanced methods, evidence with self-check reliability can assist in deciphering minor differences in hardly identifiable problems. Moreover, only evidence can provide a Bayesian model averaging method for better prediction in such problematic cases.

## 6.2 Sensitivity Analysis

A sensitivity analysis of the evidence was performed. We generated 1,024 datasets using two-RC-pair models while varying the following five parameters; the number

Table 4. Functional ANOVA results

factors	LEM	LEV	residual
$(m)$	0.0551	0.0113	0.0012
(KL)	<b>0.3255</b>	<b>0.3256</b>	<b>0.3405</b>
(SNR)	0.2336	0.2420	0.0825
$(m, \text{KL})$	0.0590	0.0163	0.0016
$(m, \text{SNR})$	0.0463	0.0802	0.2428
(KL, SNR)	0.2251	0.2338	0.0876
$(m, \text{KL}, \text{SNR})$	0.0555	0.0908	0.2438

of data  $m$ , scaling factor  $r_t$ , the first resistance  $r'_1$ , the first time constant  $\tau_1^{\text{std}}$ , and noise variance  $\sigma_{\text{noise}}$ . As these raw input parameters cannot be compared with various models, we calculated the SNR, KL, and the number of data points  $m$  for each dataset. In the first step of the analysis, we compared the linear correlations between the evidence. Table 3 shows Pearson’s correlation coefficients. This result aligns with our intuitions; for instance, larger data size  $m$  and SNR can boost the evidence LEM and confidence (inverse of LEV). However, while the largest correlation with SNR is instinctive, the small correlation with KL is counterintuitive.

Thus, we further investigated the variance analysis via functional ANOVA (Hutter et al., 2014), which models a partition of a functional response according to the main effects and interactions of input parameters. This method can attribute each parameter sensitivity in a non-linear manner. Table 4 illustrates that the most significant influence over the mean and variance of evidence is KL, contrary to the linear correlation results. This can be interpreted as a smaller KL (more overlapped peaks) destabilising the evidence estimation, resulting in a more considerable variance. This viewpoint is supported by the relatively large negative coefficient between KL and LEV.

Further insights can be obtained via residual analysis. The residual is defined as follows:

$$Z_{\text{pred}} := \text{slope} \times \text{BIC} + \text{intercept}, \quad (28)$$

$$\text{residual} := (Z_{\text{pred}} - \log \mathbb{E}_{\pi}[\mu_e(\Theta)])^2. \quad (29)$$

As BIC is an approximation of the log evidence mean, they have a linear relationship. While a linear regression model with BIC can predict log evidence mean reasonably, it fails to predict in hard cases, as shown in the section 6.1. Residual refers to the squared error between BIC and log evidence mean. Table 4 shows that the residual is mainly caused by KL and less influenced by SNR or the number of data points  $m$ . This also suggests that BIC cannot distinguish the models with overlapped peaks, namely, multimodal posterior.

## 6.3 Computation Efficiency

Lastly, we compared the computation efficiency of our modified version of BASQ to the existing MCMC solvers; elliptical slice sampling (ESS) (Murray et al., 2010) and dynamic nested sampling (Speagle, 2020). Note that amongst MCMC samplers, only nested sampling can estimate the evidence. For ESS, we approximated evidence using ELPD via posterior samples. Therefore, the estimation with ESS should converge to a larger value than the

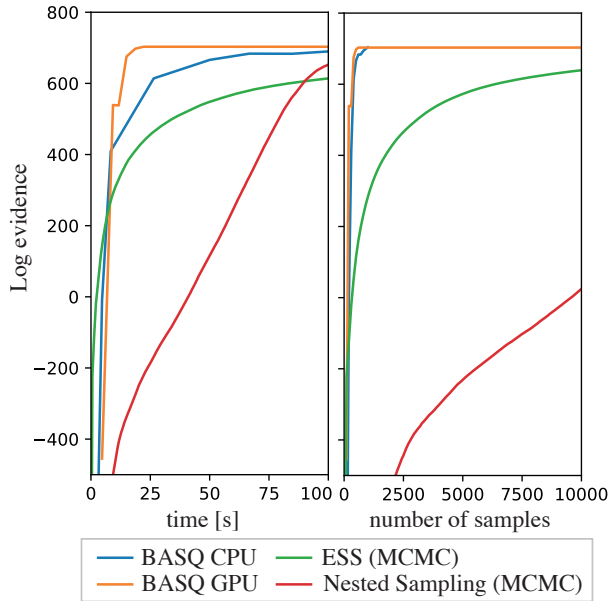


Fig. 2. The learning curve of log evidence over the computation time and the number of samples.

evidence. BASQ computation was performed using both CPU and GPU.<sup>1</sup>

Figure 2 compares the learning curve of the above four samplers with computation time, with the easy case dataset shown in Table 1. While BASQ in GPU converges at 18 seconds, BASQ in CPU converges at 131 seconds. Both ESS and nested sampling do not converge yet. Figure 2 contrasts the sample efficiency of the samplers. As BASQ is a parallel sampler, we generate 100 samples per iteration. The sampling efficiency of BASQ does not change over computation modes. The sampling efficiency of BASQ is the best of the selected solvers. This corresponds to the theory: While the convergence rate of BASQ is  $\mathcal{O}(\exp(-cn^{1/d}))$  in the Gaussian case (see Theorem 1 in Adachi et al. (2022)), the one of MCMC is  $\mathcal{O}(1/\sqrt{n})$ .

Furthermore, even this result does not fully represent BASQ’s potential. The number of parallel samples (100) exceeds the CPU cores or GPU memory capacity used in the experiments. Hence, parallelisation causes additional time compared to an ideal situation, such as a computer cluster. Moreover, this experiment adopted ECM for simplicity, which can return model prediction in a millisecond order. However, more complex models, such as the Newman model, take seconds to query. Therefore, in such complex cases, the computation time superiority of BASQ will shine even more.

## REFERENCES

Adachi, M., Hayakawa, S., Jørgensen, M., Oberhauser, H., and Osborne, M.A. (2022). Fast Bayesian inference with batch Bayesian quadrature via kernel recombination. *Advances in neural information processing systems (NeurIPS)*, 35.

<sup>1</sup> Both MCMC samplers and BASQ in CPU were computed with MacBook Pro 2019, 2.4 GHz 8-Core Intel Core i9, 64 GB 2667 MHz DDR4. BASQ in GPU was performed on Google Colaboratory.

- Aitio, A., Marquis, S.G., Ascencio, P., and Howey, D.A. (2020). Bayesian parameter estimation applied to the Li-ion battery single particle model with electrolyte dynamics. *IFAC*, 53(2), 12497–12504.
- Bizeray, A.M., Kim, J.H., Duncan, S.R., and Howey, D.A. (2018). Identifiability and parameter estimation of the single particle lithium-ion battery model. *IEEE Trans. Control. Syst. Technol.*, 27(5), 1862–1877.
- Calderwood, J. (2003). A physical hypothesis for Cole-Davidson behavior. *IEEE transactions on dielectrics and electrical insulation*, 10(6), 1006–1011.
- Chai, H.R. and Garnett, R. (2019). Improving quadrature for constrained integrands. In *The 22nd International Conference on Artificial Intelligence and Statistics*, 2751–2759. PMLR.
- Doyle, M., Fuller, T.F., and Newman, J. (1993). Modeling of galvanostatic charge and discharge of the lithium/polymer/insertion cell. *J. Electrochem. Soc.*, 140(6), 1526.
- Escalante, J.M., Sahu, S., Foster, J.M., and Protas, B. (2021). On uncertainty quantification in the parametrization of Newman-type models of lithium-ion batteries. *J. Electrochem. Soc.*, 168(11), 110519.
- Gunter, T., Osborne, M.A., Garnett, R., Hennig, P., and Roberts, S.J. (2014). Sampling for inference in probabilistic models with fast Bayesian quadrature. *Advances in neural information processing systems*, 27.
- Hastings, W.K. (1970). Monte Carlo sampling methods using Markov chains and their applications. *Biometrika*, 57(1), 97–109. URL <https://doi.org/10.1093/biomet/57.1.97>.
- Hayakawa, S., Oberhauser, H., and Lyons, T. (2022). Positively weighted kernel quadrature via subsampling. *Advances in neural information processing systems (NeurIPS)*, 35.
- He, H., Xiong, R., and Fan, J. (2011). Evaluation of lithium-ion battery equivalent circuit models for state of charge estimation by an experimental approach. *Energies*, 4(4), 582–598.
- Huang, J., Papac, M., and O’Hayre, R. (2021). Towards robust autonomous impedance spectroscopy analysis: A calibrated hierarchical Bayesian approach for electrochemical impedance spectroscopy (eis) inversion. *Electrochim. Acta*, 367, 137493.
- Hutter, F., Hoos, H., and Leyton-Brown, K. (2014). An efficient approach for assessing hyperparameter importance. In *International conference on machine learning (ICML)*, 754–762. PMLR.
- Jeffreys, H. (1998). *The theory of probability*. OUP Oxford.
- Kemper, P. and Kum, D. (2013). Extended single particle model of Li-ion batteries towards high current applications. In *IEEE VPPC*, 1–6. IEEE.
- Kitagawa, G. (1993). A Monte Carlo filtering and smoothing method for non-Gaussian nonlinear state space models. In *Proceedings of the 2nd U.S.-Japan Joint Seminar on Statistical Time Series Analysis*, 110.
- Kuhn, Y., Wolf, H., Latz, A., and Horstmann, B. (2022). EP-BOLFI: Measurement-noise-aware parameterization of continuum battery models from electrochemical measurements applied to full-cell GITT measurements. *arXiv preprint arXiv:2208.03289*.
- Liu, J. and Ciucci, F. (2020). The Gaussian process distribution of relaxation times: A machine learning

tool for the analysis and prediction of electrochemical impedance spectroscopy data. *Electrochim. Acta*, 331, 135316.

Metropolis, N., Rosenbluth, A.W., Rosenbluth, M.N., Teller, A.H., and Teller, E. (1953). Equation of state calculations by fast computing machines. *Chem. Phys.*, 21(6), 1087–1092.

Milocco, R.H., Thomas, J.E., and Castro, B. (2014). Generic dynamic model of rechargeable batteries. *J. Power Sources*, 246, 609–620.

Miyazaki, Y., Nakayama, R., Yasuo, N., Watanabe, Y., Shimizu, R., Packwood, D.M., Nishio, K., Ando, Y., Sekijima, M., and Hitosugi, T. (2020). Bayesian statistics-based analysis of ac impedance spectra. *AIP Advances*, 10(4), 045231.

Murphy, K.P. (2012). *Machine learning: a probabilistic perspective*. MIT press.

Murray, I., Adams, R., and MacKay, D. (2010). Elliptical slice sampling. In *Proceedings of the thirteenth international conference on artificial intelligence and statistics*, 541–548. JMLR Workshop and Conference Proceedings.

Osborne, M., Garnett, R., Ghahramani, Z., Duvenaud, D.K., Roberts, S.J., and Rasmussen, C. (2012). Active learning of model evidence using Bayesian quadrature. *Advances in neural information processing systems*, 25.

Rasmussen, C. and Ghahramani, Z. (2000). Occam’s razor. *Advances in neural information processing systems (NeurIPS)*, 13.

Santhanagopalan, S., Guo, Q., Ramadass, P., and White, R.E. (2006). Review of models for predicting the cycling performance of lithium ion batteries. *J. Power Sources*, 156(2), 620–628.

Speagle, J.S. (2020). dynesty: a dynamic nested sampling package for estimating Bayesian posteriors and evidences. *Monthly Notices of the Royal Astronomical Society*, 493(3), 3132–3158.

## Appendix A. BAYESIAN QUADRATURE TRAINING PROCEDURE

### A.1 Four-Layered BASQ Formulation

The likelihood surrogate model  $\ell(\Theta)$  is defined as:

$$\ell(\Theta) \sim \mathcal{N}(\ell; \mu_\ell(\Theta), \sigma_\ell(\Theta)), \quad (\text{A.1})$$

$$\mu_\ell(\Theta) = K(\Theta, \Theta)K(\Theta, \Theta)^{-1}\ell_{\text{true}}(\Theta), \quad (\text{A.2})$$

$$\sigma_\ell(\Theta, \Theta') = K(\Theta, \Theta') - K(\Theta, \Theta)K(\Theta, \Theta)^{-1}K(\Theta, \Theta'), \quad (\text{A.3})$$

where  $\ell(\Theta)$  is the surrogate likelihood function modelled by GP,  $\Theta$  is the ‘observed parameter sets’, and  $K$  is the kernel.

GP is a non-parametric probabilistic model, typically applied to regression tasks in machine learning. GP can flexibly increase the model complexity in accordance with the number of data, thwarting under/over-confidence. GP model shape is determined by the data points  $\Theta$  and the kernel  $K(\Theta, \Theta')$ . The kernel maps the correlation between data points into a covariance matrix. Gaussianity of GP provides analytical predictive distribution  $\ell(\Theta)$ , with predictive mean  $\mu_\ell(\Theta)$  and covariance  $\sigma_\ell(\Theta, \Theta')$ , as shown in Eqs (A.2) - (A.3). While the predictive mean  $\mu_\ell(\Theta)$  predicts the likelihood  $\ell_{\text{true}}(\Theta)$ , predictive covariance  $\sigma_\ell(\Theta, \Theta')$  predicts the uncertainty of the predic-

tion at given  $\Theta$ . That is, training GP means minimising the predictive covariance over all possible parameters  $\pi(\Theta)$ , namely, minimising  $\iint_{\chi} \sigma_\ell(\Theta, \Theta') d\pi(\Theta) d\pi(\Theta')$ . Such training can be done via querying more observations from the true likelihood  $\mathbf{D}_\Theta = \{\Theta, \ell_{\text{true}}(\Theta)\}$ . Hence, the most straightforward training is to sample from the prior  $\pi(\Theta)$  until the integral variance becomes smaller than a convergence threshold. However, the prior often barely overlaps over the likelihood, resulting in observing unhelpful tiny likelihood values over most samples.

To overcome this problem, we consider sample-efficient training that fully exploits the information from GP. Osborne et al. (2012) showed that active learning sampling could efficiently reduce the number of samples. The active learning scheme guides the next query point to minimise the integral variance, exploiting the GP surrogate model information. A function called acquisition function formulated by predictive mean  $\mu_\ell(\Theta)$  and covariance  $\sigma_\ell(\Theta, \Theta')$  can evaluate where to sample, and optimising it can locate where to sample next. Still, the overhead of the next query guidance is not negligible, and it is an inevitably sequential procedure. Adachi et al. (2022) proposed batch Bayesian quadrature, termed Bayesian Alternately Sub-sampled Quadrature (BASQ), permitting a lightweight active learning scheme and parallelisation of querying. They adopted the discretised sampling method (Hayakawa et al., 2022) for probability measure rather than an acquisition function. This allows us to query the true function in parallel. As the modern computational environment exploits an efficient parallel computation via a graphical processing unit or a computer cluster in the cloud, such computing power can accelerate inference computation. They demonstrated that BASQ could accelerate Bayesian inference over various synthetic and real-world datasets, including SPMe model inference.

The evidence can be calculated via kernel recombination. Kernel recombination is a discrete approximation of continuous kernel integral into weighted summation so as to minimise the integral variance, as such:

$$\int_Q \varphi(x) dq(x) \approx \sum_p^P w_p \varphi(X_p), \\ X_p \in \mathbf{X}, w_p \in \mathbf{W},$$

$\mathbf{X}$  is the discretised samples over the probability measure,  $\mathbf{W}$  is the positive weights to approximate integration. When we recall our training objective is to minimise the predictive covariance over the probability measure  $\pi(\Theta)$ , this can be formulated as kernel recombination. Hence, we pass the predictive covariance  $\sigma_\ell(\Theta, \Theta')$  as kernel to the kernel recombination algorithm (Hayakawa et al., 2022), which yields the following approximation:

$$\mathbf{X}, \mathbf{W} = \text{recombination}[\sigma_\ell(\Theta, \Theta'), \pi(\Theta)], \\ \mathbb{E}_\pi[\ell(\Theta)] = \int_{\chi} \mu_\ell(\Theta) d\pi(\Theta), \\ \approx \sum_k^L W_k \mu_\ell(X_k),$$



Table A.1. Four-layered GPs and warped functions at each layer

Layers	$e$ space	$f$ space	$g$ space	$h$ space
Correspondence	likelihood	normalised likelihood	square-root norm. likelihood	sqrt. norm. log likelihood
Warp	scaling	square-root	log	base GP
Forward	$e$	$e/\exp \beta$	$\sqrt{2(f-\alpha)}$	$\log(g+1)$
Backward	$f \exp \beta$	$\alpha + \frac{1}{2}g^2$	$\exp(h) - 1$	$h$
GP	$e \sim \mathcal{GP}(\mu_e, \sigma_e)$	$f \sim \mathcal{GP}(\mu_f, \sigma_f)$	$g \sim \mathcal{GP}(\mu_g, \sigma_g)$	$h \sim \mathcal{GP}(\mu_h, \sigma_h)$
Mean	$\mu_f(x) \exp \beta$	$\alpha + \frac{1}{2} [\mu_g(x)^2 + \sigma_g(x, x)]$	$\exp [\mu_h(x) + \frac{1}{2}\sigma_h(x, x)]$	$\mu_h(x)$
Covariance	$\sigma_f(x, y) \exp(2\beta)$	$\frac{1}{2}\sigma_g(x, y)^2 + \mu_g(x)\sigma_g(x, y)\mu_g(y)$	$\mu_g(x)\mu_g(y)[\exp\{\sigma_h(x, y) - 1\}]$	$\sigma_h(x, y)$

$$\begin{aligned} \text{Var}_\pi[\ell(\Theta)] &= \iint_{\chi} \sigma_\ell(\Theta, \Theta') d\pi(\Theta) d\pi(\Theta'), \\ &\approx \sum_{k,l}^L W_k W_l \sigma_\ell(X_k, X_l), \end{aligned}$$

where  $X_k, X_l \in \mathbf{X}$ ,  $W_k, W_l \in \mathbf{W}$ . However, they adopted square-root warping for fast computation, which assumed a narrow dynamic range in likelihood. Battery models' likelihood turns out to be very sharp, as the number of data points over the frequency range is typically over a hundred.

Therefore, we adopted four-layered GPs to accommodate the dynamic range, permitting solving Bayesian inference even in this wide dynamic range case. Functions at each layer are summarised in Table A.1, where  $\mathbf{Y}_{\log}$  is the observed log-likelihood values,  $\alpha = \min[\exp(\mathbf{Y}_{\log} - \beta)]$ ,  $\beta = \max[\mathbf{Y}_{\log}]$ .  $e$  space corresponds to the original likelihood space. Square-root warping and log-warping layers are approximated via the moment-matching method (Gunter et al., 2014; Chai and Garnett, 2019). To accommodate the wide dynamic range, log transformation is widely applied in the BQ community. However, log-warped GP inevitably results in sampling from log space, leading to ineffective exploration. As meaningful samples from a very sharp likelihood are localised in only the vicinity of the maximum values, log space exploration is too blunt to explore the original space. The combination of square-root warping and log-warping can overcome this issue using the following relationship:

$$\begin{aligned} f &= \alpha + \frac{1}{2}g^2 \approx \alpha + \frac{1}{2} \exp(h) \exp(h), \\ \mathbb{E}_\pi[\mu_f(\Theta)] &= \alpha + \frac{1}{2} \int_{\Xi} \mu_g(\Theta) d\pi'(\Theta), \\ \pi'(\Theta) &:= \mu_g(\Theta) \pi(\Theta). \end{aligned}$$

As such, this doubly warping structure enables us to copy exponentiated function information to both likelihood and prior. Thus, this double structure can sample from sharp exponentiated distribution  $\pi'(\Theta)$  as well as keep the surrogate model exponentiated  $\mu_g(\Theta)$ .

The last layer,  $e$ , exists to avoid overflow in computation by scaling the whole dynamic range via maximum value. This warping layer can be avoided as such:

$$\begin{aligned} \log \mathbb{E}_\pi[\mu_e(\Theta)] &= \log \mathbb{E}_\pi[\mu_f(\Theta)] + \beta, \\ &\approx \log \sum_k^L W_k \mu_f(X_k) + \beta, \end{aligned}$$

$$\log \text{Var}_\pi[\sigma_e(\Theta)] = \log \text{Var}_\pi[\sigma_f(\Theta)] + 2\beta,$$

$$\approx \log \sum_{k,l}^L W_k W_l \sigma_f(X_k, X_l) + 2\beta,$$

$$p(\Theta|\mathbf{D}, M) = \frac{\mu_e(\Theta)\pi(\Theta)}{\mathbb{E}_\pi[\mu_e(\Theta)]} = \frac{\mu_f(\Theta)\pi(\Theta)}{\mathbb{E}_\pi[\mu_f(\Theta)]}.$$

## A.2 Training Procedures

Training consists of four processes:

- (1) Subsampling from the exponentiated distribution
- (2) Kernel recombination for batch sampling
- (3) GP hyperparameter optimisation
- (4) Evidence estimation

We iterate the above four procedures until the evidence variance reaches plateau. Only the first training procedure is different from the original BASQ (Adachi et al., 2022).

The subsampling is to sample from the prior distribution to construct the empirical measure. As the kernel recombination is to select the sparse sample set from subsamples that can minimise the integral variance, subsamples should be sampled from prior but well overlapped from the higher predictive variance of GP  $\ell(x)$ . Adachi et al. (2022) adopted uncertainty sampling for faster convergence, which samples from predictive variance  $\sigma_\ell(x)$  and corrected to prior distribution via importance sampling, as such:

$$\begin{aligned} g_{\text{prop}}(\Theta) &:= (1-r)\mu_g(\Theta) + r\tilde{A}(\Theta), \quad 0 \leq r \leq 1 \\ w_{\text{IS}}(\Theta) &:= \mu_g(\Theta)/g_{\text{prop}}(\Theta), \\ \tilde{A}(\Theta) &:= \sigma_g(\Theta)\pi'(\Theta)/Z_{\tilde{A}}, \\ Z_{\tilde{A}} &:= \int_{\Xi} \sigma_g(\Theta) d\pi'(\Theta), \\ \sigma_g(\Theta) &:= \text{diag}[\sigma_g(\Theta, \Theta)]. \end{aligned}$$

We wish to adopt the same strategy for a four-layered GP, but the log-warp layer hinders the application. The predictive variance of the original BASQ can be analytically translated into the mixture of Gaussian with Gaussian kernel because the squared Gaussian distribution is still Gaussian. However, the exponentiated Gaussian is no more



Table A.2. Ablation study of warped layers

log	square-root	scaling	LEM	LEV
✓			overflow	overflow
	✓		overflow	overflow
		✓	361.8172	-11.90735
✓		✓	677.8633	-21.86860
	✓	✓	449.6425	-13.13063
✓	✓	✓	<b>703.6569</b>	-27.31169

Gaussian, which becomes a log-normal distribution. As such, we cannot take the same strategy which exploits the Gaussianity. Hence, we employ the heuristical method. The predictive variance is expected to be larger at the midpoints between the observed data points. Thus, sampling from the midpoints with half lengthscale of GP is expected to be good proposal distribution of sampling the uncertainty region, as such:

$$g_{\text{heur}}(\Theta) := \sum_{r,s}^{N_{\text{heur}}} w_{r,s}^{\text{heur}} \mathcal{N}\left(\Theta; \Theta_{r,s}^{\text{mid}}, \frac{\mathbf{W}_{\text{length}}}{2}\right),$$

$$\Theta_{r,s}^{\text{mid}} := \frac{\Theta_r + \Theta_s}{2},$$

$$w_{r,s}^{\text{heur}} := \frac{\sigma_g(\Theta_{r,s}^{\text{mid}}) \pi'(\Theta_{r,s}^{\text{mid}})}{\sum_{r,s}^{N_{\text{heur}}} \sigma_g(\Theta_{r,s}^{\text{mid}}) \pi'(\Theta_{r,s}^{\text{mid}})},$$

where  $\Theta_r, \Theta_s \in \Theta$  are the observed parameters,  $\mathbf{W}_{\text{length}}$  is the diagonal covariance matrix whose diagonal elements are the lengthscales of each dimension. Supersampling from this offers the uncertainty sampling, as such:

$$\Theta_t^{\text{super}} \sim g_{\text{heur}}(\Theta) \in \mathbb{R}^{N_{\text{super}}},$$

$$Z_{\tilde{A}} = \int \sigma_g(\Theta) \frac{\pi'(\Theta)}{g_{\text{heur}}(\Theta)} d g_{\text{heur}}(\Theta),$$

$$\approx \frac{1}{N_{\text{super}}} \sum_t^{N_{\text{super}}} \sigma_g(\Theta_t^{\text{super}}) \frac{\pi'(\Theta_t^{\text{super}})}{g_{\text{heur}}(\Theta_t^{\text{super}})},$$

$$w^{\text{super}} := \tilde{A}(\Theta_t^{\text{super}}) / g_{\text{heur}}(\Theta_t^{\text{super}}).$$

Sequential Monte Carlo (Kitagawa, 1993) permits to sample from  $\tilde{A}(\Theta)$ .

### A.3 Ablation study of layered GPs

We discuss the efficacy of four-layered GP by comparing the results of evidence inference for the easy case introduced in Table 1. We compared the following six configurations in Table A.2. The ground truth of LEM is estimated via exhaustive nested sampling with millions of samples until convergence, which yields 703.7285. The ablation study shows that the four-layered GPs can estimate the most accurate LEV of all compared configurations. GPs without the scaling layer reached the overflow limit, which returned a positive infinite value. GPs without the logarithmic layer scored the lower log evidence mean because the surrogate model cannot accommodate the wide dynamic range. Scaled GP with only log warp results was the second best. However, the non-exponentiated prior

struggled to find the MAP location. As such, the four-layered GP, employing all features, was the performant.

## Appendix B. IDENTIFIABILITY DERIVATION

### B.1 Hyperbolic Secant Distribution Identities

$$\int_{-\infty}^{\infty} \text{sech}(x) dx = \pi, \quad (\text{B.1})$$

$$\int_{-\infty}^{\infty} \text{sech}\left(\frac{x-a}{b}\right) dx = \frac{\pi}{b}, \quad (\text{B.2})$$

$$\int_{-\infty}^{\infty} \text{sech}(x) \ln \text{sech}(x) dx = -\pi \ln 2, \quad (\text{B.3})$$

$$\int_{-\infty}^{\infty} \text{sech}(x) \text{sech}(x-a) dx = 2 \text{acsch}(a), \quad (\text{B.4})$$

$$\int_{-\infty}^{\infty} \text{sech}(x)^2 dx = 2. \quad (\text{B.5})$$

### B.2 SNR Derivation

$$\text{SNR} := \ln \frac{\text{Var}_{P(\ln \omega)}[\text{Im}[Z]]}{\sigma_{\text{noise}}},$$

$$\text{Var}_{P(\ln \omega)}[\text{Im}[Z]] = \mathbb{E}_{P(\ln \omega)}[\text{Im}[Z]^2] - \mathbb{E}_{P(\ln \omega)}[\text{Im}[Z]]^2,$$

$$\mathbb{E}_{P(\ln \omega)}[\text{Im}[Z]] = \int_{\Omega} \text{Im}[Z](\ln \omega) dP(\ln \omega),$$

$$= \frac{\exp(r_t) \pi (1 - r_0)}{2(b-a)},$$

$$\mathbb{E}_{P(\ln \omega)}[\text{Im}[Z]^2] = \frac{\exp(2r_t) (1 - r_0)^2}{2(b-a)} A,$$

where

$$P(\ln \omega) := \mathcal{U}(\ln \omega; a, b),$$

$$a, b := \min[\ln \omega], \max[\ln \omega],$$

$$A := \sum_i^N w_i^2 + \sum_{i,j}^N 2w_i w_j \Delta \tau_{ij} \text{csch}(\Delta \tau_{ij}),$$

$$\Delta \tau_{ij} := \sigma_{\omega}(\tau_i^{\text{std}} - \tau_j^{\text{std}}).$$

Eq. (B.2) yields the analytical solution of the first expectation:

$$\mathbb{E}_{P(\ln \omega)}[\text{Im}[Z]] = \int_{\Omega} P(\text{Im}[Z]|\omega) dP(\omega),$$

$$= \frac{\exp(r_t) \pi (1 - r_0)}{2(b-a)} \sum_{i=1}^N \frac{w_i}{\pi}$$

$$\int_{-\infty}^{\infty} \text{sech}(\omega + \Delta \tau_{ij}) d\omega,$$

$$= \frac{\exp(r_t) \pi (1 - r_0)}{2(b-a)} \sum_{i=1}^N w_i,$$

$$= \frac{\exp(r_t) \pi (1 - r_0)}{2(b-a)}.$$

Eqs. (B.4) - (B.5) yield the analytical solution of the second expectation:

$$\begin{aligned}
\mathbb{E}_{P(\ln \omega)}[\text{Im}[Z]^2] &= \int_{\Omega} P(\text{Im}[Z]|\omega)^2 dP(\omega), \\
&= \frac{1}{b-a} \left[ \frac{\exp(r_t)\pi(1-r_0)}{2} \right]^2 \\
&\quad \int_{-\infty}^{\infty} \left[ \sum_{i=1}^N \frac{w_i}{\pi} \text{sech}(\omega + \Delta\tau_{ij}) \right]^2 d\omega, \\
&= \frac{1}{b-a} \left[ \frac{\exp(r_t)\pi(1-r_0)}{2} \right]^2 \\
&\quad \int_{-\infty}^{\infty} \left[ \sum_i^N \frac{w_i^2}{\pi^2} \text{sech}(\omega + \Delta\tau_{ij})^2 + \right. \\
&\quad \left. \sum_{i,j}^N \frac{2w_i w_j}{\pi^2} \text{sech}(\omega) \text{sech}(\omega + \Delta\tau_{ij}) \right] d\omega, \\
&= \frac{1}{b-a} \left[ \frac{\exp(r_t)\pi(1-r_0)}{2} \right]^2 \\
&\quad \left\{ \sum_i^N \frac{2w_i^2}{\pi^2} + \sum_{i,j}^N \frac{4w_i w_j}{\pi^2} \Delta\tau_{ij} \text{csch}(\Delta\tau_{ij}) \right\}, \\
&= \frac{\exp(2r_t)(1-r_0)^2}{2(b-a)} \\
&\quad \left\{ \sum_i^N w_i^2 + \sum_{i,j}^N 2w_i w_j \Delta\tau_{ij} \text{csch}(\Delta\tau_{ij}) \right\}.
\end{aligned}$$

$g_{\text{KL}}(x)$  is a proposal distribution. As the logarithmic term is a subtraction of two hyperbolic secant distributions, the peak is estimated around the overlapped area, namely the midpoint of the two peaks  $x + \sigma_{\omega} w_i \tau_i^{\text{std}} + 0.5\Delta_{ij}$ . We can solve this integral via Monte Carlo integration. As sampling and evaluation of the probability density function of hyperbolic secant distribution are done within a millisecond order, computation with millions of samples for accuracy is not demanding.

### B.3 KL derivation

The asymmetric  $\text{KL}_{i|j}$  and symmetric KL definitions are as follows:

$$\begin{aligned}
\text{KL}_{i|j} &:= \int_P \ln \left( \frac{P_i(x)}{P_j(x)} \right) dP_i(x), \\
\text{KL} &:= \text{KL}_{i|j} + \text{KL}_{j|i}.
\end{aligned}$$

To incorporate the information of weights, we adopt the following scaled hyperbolic secant distributions:

$$\begin{aligned}
P_i(\ln \omega) &:= \frac{w_i}{\pi} \text{sech} [w_i(\ln \omega + \sigma_{\omega} \tau_i^{\text{std}})], \\
P'_j(\ln \omega) &:= \frac{w_j}{\pi} \text{sech} [w_j(\ln \omega + \sigma_{\omega} \tau_j^{\text{std}})],
\end{aligned}$$

where  $\tau_j^{\text{std}} > \tau_i^{\text{std}}$ . For efficient computation of the integrals, we can adopt the importance sampling, as such:

$$\begin{aligned}
\text{KL}_{i|j} &= \int_P \frac{P_i(x)}{g_{\text{KL}}(x)} \ln \frac{P_i(x)}{P_j(x)} dg_{\text{KL}}(x), \\
X_q^{\text{IS}} &\sim g_{\text{KL}}(x) \in \mathbb{R}^{N_{\text{IS}}}, \\
\text{KL}_{i|j} &\approx \frac{1}{N_{\text{IS}}} \sum_q \frac{P_i(X_q^{\text{IS}})}{g_{\text{KL}}(X_q^{\text{IS}})} \ln \frac{P_i(X_q^{\text{IS}})}{P_j(X_q^{\text{IS}})},
\end{aligned}$$

where

$$\begin{aligned}
g_{\text{KL}}(x) &:= \frac{1}{2N} \sum_i^N \frac{w_i}{\pi} \text{sech} [w_i(x + \sigma_{\omega} \tau_i^{\text{std}})] \\
&\quad + \frac{1}{4\pi} \text{sech} [0.5(x + \sigma_{\omega} w_i \tau_i^{\text{std}} + 0.5\Delta_{ij})], \\
\Delta_{ij} &:= \sigma_{\omega} |w_j \tau_j^{\text{std}} - w_i \tau_i^{\text{std}}|,
\end{aligned}$$